

Impact of printed wiring board coatings on the reliability of lead-free chip-scale package interconnections

T.T. Mattila, V. Vuorinen, and J.K. Kivilahti

*Laboratory of Electronics Production Technology, Helsinki University of Technology,
02150 Espoo, Finland*

(Received 27 February 2004; accepted 12 July 2004)

When lead-free solder alloys mix with lead-free component and board metallizations during reflow soldering, the solder interconnections become multicomponent alloy systems whose microstructures cannot be predicted on the basis of the SnPb metallurgy. To better understand the influences of these microstructures on the reliability of lead-free electronics assemblies, SnAgCu-bumped components were reflow-soldered with near-eutectic SnAgCu solder pastes on Ni(P)|Au- and organic solderability preservative (OSP)-coated printed wiring boards and tested under cyclic thermal shock loading conditions. The reliability performance under thermomechanical loading was found to be controlled by the kinetics of recrystallization. Because ductile fracturing of the as-soldered tin-rich colonies would require a great amount of plastic work, the formation of continuous network of grain boundaries by recrystallization is needed for cracks to nucleate and propagate intergranularly through the solder interconnections. Detailed microstructural observations revealed that cracks nucleate and grow along the grain boundaries especially between the recrystallized part and the non-recrystallized part of the interconnections. The thermal cycling test data were analyzed statistically by combining the Weibull statistics and the analysis of variance. The interconnections on Ni(P)|Au were found out to be more reliable than those on Cu|OSP. This is due to the extensive dissolution of Cu conductor, in the case of the Cu|OSP assemblies, into molten solder that makes the microstructure to differ noticeably from that of the Ni(P)|Au interconnections. Because of large primary Cu_6Sn_5 particles, the Cu-enriched interconnections enhance the onset of recrystallization, and cracking of the interconnections is therefore faster. The solder paste composition had no statistically significant effect on the reliability performance.

I. INTRODUCTION

Constant demands for greater functionality and better performance of consumer electronics are driving electronics manufacturers to continue the integration and miniaturization of their products. This trend will increase electrical interconnection densities and decrease solder volumes and thereby add significantly to the strains and stresses experienced by solder interconnections. Furthermore, the recent requirements for environmentally friendly electronics production are creating new complications in the adoption of lead-free solders and component and board metallizations. A major consequence of moving to lead-free electronics production is the employment of a large number of new lead-free material combinations, the metallurgical compatibility of which is not yet well established.^{1,2} The change to lead-free electronics production could have an important effect especially

on the reliability of portable electronics, which experience accidental shock loadings, strong local heating of power components, and varying operational environments.

Chip-scale packages (CSP) and small ball grid arrays (BGA) are widely used in portable electronics equipment, and their performance under thermal shock loading has been widely studied.³⁻⁹ The emphasis in most recent papers has been on the difference in thermal fatigue life between assemblies soldered with lead bearing and lead-free alloys. The unanimous conclusion seems to be that the lead-free assemblies yield better fatigue life than those manufactured with SnPb solders. Only a few studies have incorporated the printed wiring board (PWB) coating materials as a factor that may affect reliability and, furthermore, the results have been inconsistent. Bradley et al.⁸ compared the reliability performance of small-scale BGA components that had been soldered either on electrolessly coated Ni|Au pads or on pads coated with organic solderability preservative (OSP). No difference in reliability was found. Another group⁹ found

significant differences, however. The different experimental setups of the two different groups may be the reason for this inconsistency. Vianco¹⁰ has presented an extensive overview of surface finishes and their role in solderability and solder interconnection performance, but he claims that the effect of surface finish dissolving into the solder interconnection is insignificant due to the relatively low rates of dissolution of traditional surface finishes (e.g., Ni, Cu, and Fe) into molten solders. None of the studies mentioned above discussed the implications of coating material dissolution into the interconnections during soldering and the possible impact of this on the microstructures and subsequent reliability.

It is well-known that the molten solder is also alloyed with the dissolving board metallization and that the dissolution can potentially degrade the performance of the solder interconnections due to the subsequent changes in the microstructures.^{11–17} Bader¹⁶ carried out an extensive study of the dissolution kinetics of the most common metallizations in the case of SnPb (60/40) solders and concluded that Ni and Pd provide the best protective finish for soldering applications. The effect of Cu dissolution on the microstructure of eutectic SnAg alloy has been studied by Chada et al.¹⁷ They found the volume fractions of the primary Sn and Cu₆Sn₅ to increase with time above liquidus and explained this in terms of the increase in Cu concentration due to the dissolution. It is clear that the amount of Cu₆Sn₅ is increased, but it is not obvious why the amount of primary Sn would increase due to Cu dissolution as is suggested by the authors. It should be noted that all the studies have been carried out with solder volumes considerably larger than those of CSP interconnections. Furthermore, the impact of the microstructural differences on the reliability of the small-scale CSP interconnections has not yet been investigated.

In this paper, the effect of solder pastes and printed wiring board protective coatings on the reliability of CSP interconnections will be investigated under fatigue stressing. The reliability of lead-free CSP interconnections was studied by employing a large number of test structures assembled in a full-scale production line, which enabled comprehensive statistical analysis. After assembly, the test boards were inspected and subjected to thermal shock testing. Detailed microstructural studies were carried out to detect the relation between the different failure mechanisms and the values of the Weibull shape parameter and thereby account for the observed differences in reliability.

II. EXPERIMENTAL

The high-density multilayer FR4 boards with four Cu layers were manufactured by the Aspocomp Group (Finland) with two different protective coatings on the Cu pads: Ni(P)|Au (Ni: 2 μm, Au: ~0.02 μm, 9 wt% P in Ni)

and OSP (0.2–0.5 μm). The test board dimensions were 43 mm × 115 mm × 1.6 mm. The component used in the study was a lead-free SnAgCu-bumped CSP component with 144 bumps (500 μm in diameter) and bump pitch of 800 μm. The height of the bumps was 480 μm and the under-bump metallurgy (UBM) consisted of ~0.6–0.8-μm-thick electrochemical Ni, on top of which there originally was a thin gold layer before bumping. The printed wiring board (PWB) pad diameter was 400 μm (non-solder mask defined). The structure of the interconnections is presented in Fig. 1. The boards were assembled using three different Pb-free no-clean solder pastes. The solder paste compositions (wt%) were Sn4.0Ag0.5Cu, Sn3.8Ag0.7Cu, and Sn3.5Ag0.75Cu, later on referred to as P₁, P₂, and P₃, respectively. In addition, the Sn36.0Pb2.0Ag alloy was used as a reference.

The solder paste was printed (DEK 265 Horizon, U.K.) with a 120-μm-thick laser cut stencil and metal squeegees, the mounting machine (Philips ACM Micro, The Netherlands) was optimized for best possible accuracy ($\mu + 5\sigma < 30 \mu\text{m}$, $C_{pk} = 1.67$), and the reflow was carried out in a conventional forced convection oven (EPM/Heraeus EWOS 5.1 N₂, Germany) under air atmosphere. The peak temperature on top of the PWB underneath the CSP component was measured with thermocouples (ECD Super M.O.L.E. Gold, Oregon) and it varied between 240 and 245 °C. The time above 217 °C was about 40–45 s depending on the profile required by the solder paste.

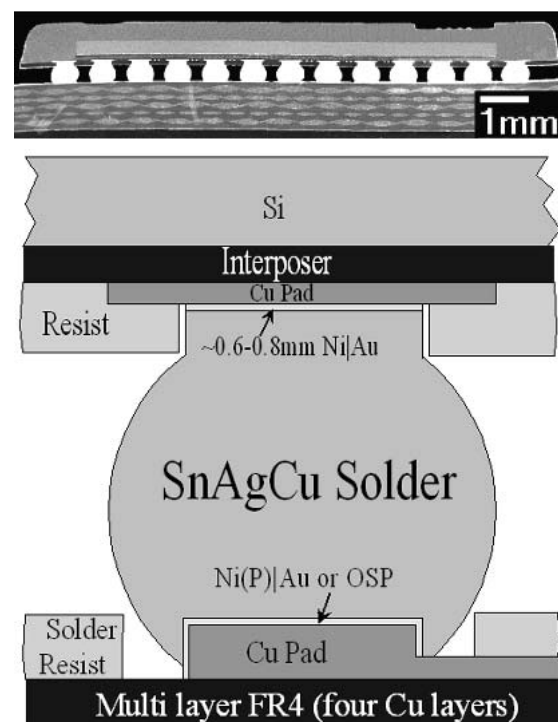


FIG. 1. Structure of the CSP package and interconnections.

After the post-reflow inspections, the assemblies were thermally cycled (Weiss TS 130, Germany) according to the IEC 68-2-14N standard (+125 °C/-45 °C, with 15 min dwell time) until all components had failed. The daisy-chain resistance measurements were performed at 125 °C in each cycle with a fixed data-logger. The criterion for failure was defined as 20% increase in the initial resistance (~24 Ω) from that after the reflow (Fig. 2).

The failure modes were studied from cross sections prepared by the standard metallographic techniques. The cross sections were analyzed by scanning electron microscopy (LEO 1450, Germany) and optical light microscopy (Olympus BX60, Japan). Polarized light was used in the optical microscopy because the reflection is dependent on grain orientation and thus differently oriented grains appear in the optical micrographs in different colors. The amount of dissolved Cu in the interconnections was measured by field emission scanning electron microscope and dispersive spectrometer (FE-SEM/EDS, JEOL 6335F, Japan) in cross-sectional samples. For the dissolution measurements, a special test board without wiring was fabricated, which showed the reference level of the topmost Cu layer (Fig. 3). The soldering pads were formed on the test boards with properly designed openings in the soldering preservative. The assemblies were subsequently produced using the same settings in each process step as with the boards assembled for the reliability tests. The amount of the dissolved copper layer was measured in interconnections of several different boards. The dissolution rate was calculated from the height loss of the Cu. The dissolved area of the cross section was determined by integration from the corner of the cross section toward the center of the pad, after which the average dissolved height was calculated. The impact of Cu dissolution on the composition of the solder interconnections was calculated from the nominal compositions of the solder and the bump alloys, their

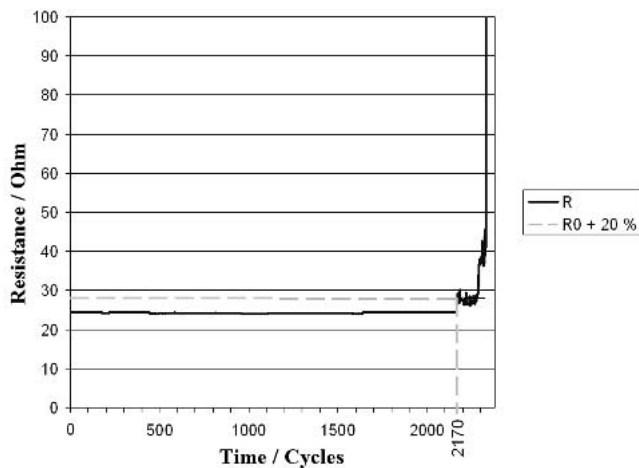


FIG. 2. Resistance plot as a function of number of cycles.

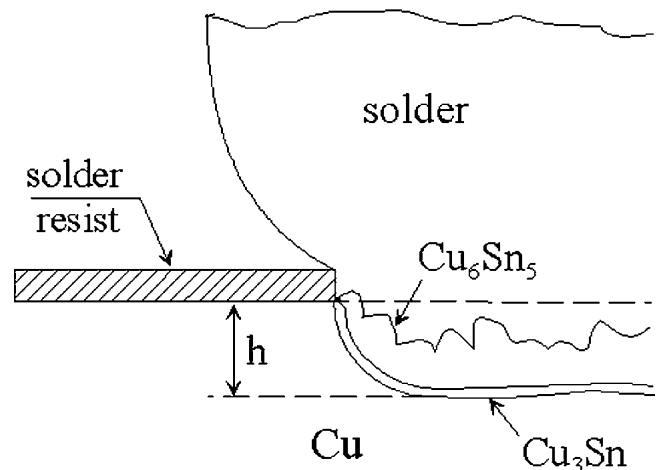


FIG. 3. Measurement principle for the Cu dissolution.

densities and volumes, the metal content of the solder pastes, and the flux densities.

The reliability test procedure was constructed as a full factorial design with seven replications. The type of lead-free *solder paste* and the *PWB coating* were the main variables. A factorial experiment, which is a series of experiments carried out according to the principles of experimental design, allows investigation of the main and interaction effects of the variables and the determination of the statistical significance of the effects. In full factorial design, all possible combinations of the factor levels are used. By replicating experiments an estimate of the experimental error can be given, which is the basic measure for determining whether the observed differences in the data are statistically significant.

Comparisons were carried out with analysis of variance (ANOVA). In ANOVA, the total variation (SS_{Tot}) in a response is subdivided into components that can be attributed to recognizable sources of variation (SS_{Levels}). Some of the variability can be explained with the use of different factor levels. The rest is due to random fluctuation within the same factor level (SS_E). The variation is quantified by the sum of squares identity, which can be written as $SS_{Tot} = SS_{Levels} + SS_E$. If there are differences in the means, most of the variation in the response is expected to be due to the different levels of the factor, that is, to SS_{Levels} . The ANOVA procedure uses this principle of comparing the significance of the difference between the SS_{Levels} and SS_E via an appropriate F ratio to test the null hypothesis of equal treatment means. The analysis yields a p-value, which is the risk level (α) for rejecting the null hypothesis of equal averages.

The reliability of the solder interconnections was studied by employing the statistical Weibull reliability analysis. The three-parameter cumulative Weibull distribution function is given by

$$F(t) = 1 - \exp \left[- \left(\frac{t - \gamma}{\eta} \right)^\beta \right],$$

where $F(t)$ is the cumulative density function, η is the characteristic lifetime, β is the shape parameter, and γ is the failure-free lifetime or the location parameter. For estimation of the parameters, the equation is written in the form $\log_{10}\ln(1/1 - F(t)) = \beta\log_{10}(t) - \beta\log_{10}(\eta)$, which is a straight line in a logarithmic timescale. The slope is then equal to β and it is estimated by the least squares regression. The η can be estimated from the intercept of the y axis, which is equal to $-\beta\ln(\eta)$. If the data points fit well to the linear assumption, the parameters can be adequately estimated using the two-parameter distribution where $\gamma = 0$. If the fit is insufficient, the two-parameter distribution may not give the most accurate results, and the presence of failure-free time (γ) or mixed failure modes should be considered. It should be noted that the η values cannot be used for statistical testing, and the significance testing is carried out instead with the average value and the variance from the seven replications.

III. RESULTS AND DISCUSSION

Results from thermal cycling tests, presented with the help of Weibull parameters, are shown in Table I. After analysis of the reliability data with ANOVA, it was concluded that there were no statistically significant differences between the CSP assemblies soldered with the different solder pastes ($\alpha < 0.001$). The compositions depart from each other insignificantly after the solder from the paste is mixed with the solder from the bumps during the assembly reflow. The composition of the bump is thus dominant; most of the solder material in the interconnection originates from the component bump and only about 10%, by volume, from the solder paste.

The bump composition was analyzed by the atomic emission/absorption spectroscopy (AES/AAS): AES (Variant Liberty, Palo Alto, CA) for Sn, and AAS (Variant 600) for Ag and Cu. The AES/AAS results indicated very high Sn content, Sn0.2Ag0.4Cu, which is exceptionally Sn rich. Because the composition of the solder bumps is close to pure tin, the two-phase region is relatively large. The calculated liquidus temperature for this composition is close to 230 °C.¹⁸ The results of the phase equilibrium calculations were verified by differential scanning calorimetry (Mettler Toledo Star DSC 821, Switzerland) measurements, which gave 229 °C for the liquidus temperature.

TABLE I. η and β values for the chip-scale packages (CSPs) soldered on Ni(P)|Au and organic solderability preservative (OSP)-coated soldering pads.

	Sn4.0Ag0.5Cu	Sn3.8Ag0.7Cu	Sn3.5Ag0.75Cu	η (combined)	β
Ni P Au	1827	2040	1980	1937	3.47
OSP	1525	1649	1257	1485	4.72

The composition of the solder interconnections can be estimated from the metal contents of the solder pastes, the flux densities, the bump volume, the nominal compositions of the bumps, and the solder pastes. Perfect filling and perfect release of the solder paste from the stencil apertures was assumed. The nominal compositions of the interconnections, when the bumps have been mixed with the solder paste alloys P₁, P₂, P₃, each individually, are Sn0.5Ag0.4Cu, Sn0.5Ag0.5Cu, and Sn0.4Ag0.4Cu, respectively. The compositions of the solders and the bump material as well as the nominal interconnection compositions after the reflow are presented in Fig. 4, which presents the Sn-rich corner of the SnAgCu phase diagram with isothermal lines representing the liquidus temperatures. P₁–P₃ represent the nominal compositions of the three solder pastes, and B is the original composition of the component bump.

Because the differences in the chemical compositions of the interconnections were found to be negligible, the effect of the pastes was ignored in the subsequent Weibull analysis. In the following, all the interconnections are assumed to have the same uniform composition of Sn0.5Ag0.5Cu after the solder paste and solder bumps are mixed together at the reflow. The Weibull plot drawn from the thermal shock results is presented in Fig. 5. Taking the failure-free life (γ) into account did not improve the analysis. The characteristic lifetimes (η) for the Ni(P)|Au and Cu|OSP are 1937 and 1485 cycles, respectively. The ANOVA shows that the difference between the average times-to-failure is significant at less than 0.05% risk level.

The Weibull distribution shape parameter (β) values for Ni(P)|Au and Cu|OSP are 3.47 and 4.72, respectively. The β value is related to the failure rate of the test

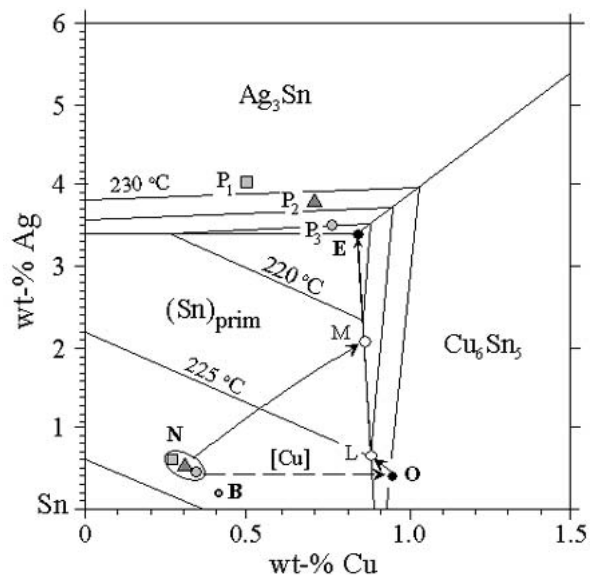


FIG. 4. Compositions of different materials and the solidification path.^{18,22}

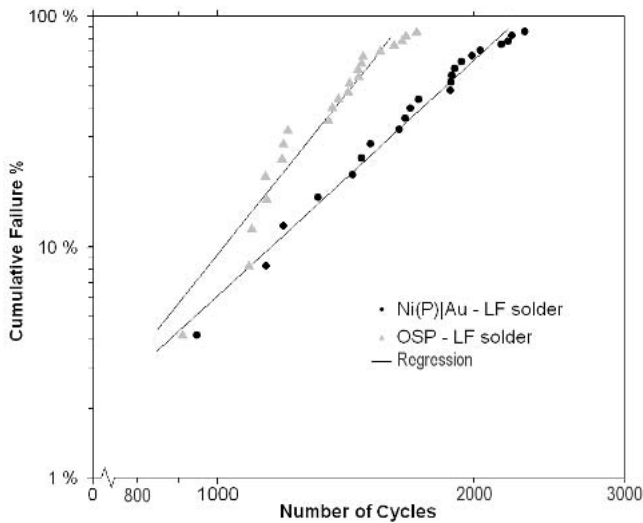


FIG. 5. Weibull reliability plots of CSPs on different coatings.

specimens and thus it is expected to correlate with a specific failure mechanism.¹⁹ The significance of the difference in β values for the two assemblies was studied by calculating the 95% confidence interval ($L_{\beta(95\%)}$) for the difference in the β values. The results show that $L_{\beta(95\%)} = 1.94 \pm 0.16$ and thus the difference is significant at less than 5% risk level. The Weibull analysis thus suggests differences in failure mechanisms for the Ni(P)|Au and OSP|Cu assemblies.

Failure analysis carried out after reliability testing revealed that in most cases the cracks had nucleated and propagated on the component side, whereas only slight cracking was observed on the PWB side of the solder interconnection. The cracks in the assemblies soldered on the Ni(P)|Au-finished boards typically nucleated and propagated in the solder material along or very close to the $(\text{Cu},\text{Ni})_6\text{Sn}_5$ layer on the component side, whereas in the assemblies soldered on Cu|OSP they typically located in the bulk solder further away from the $(\text{Cu},\text{Ni})_6\text{Sn}_5$ |solder interface of the component (Figs. 6 and 7). Other than that, the failure modes appeared to be closely similar. No other failure modes were detected.

Because solder pastes did not affect the reliability performance but the coating materials did, the differences in the microstructures were studied in detail. The microstructural analysis carried out on the cross-sectional samples of the component interconnections, before they were soldered to the substrate, revealed that the original Au finish on Ni had dissolved completely into the solder bump during the bumping of the components. In the reflow bumping, when the molten SnAgCu solder comes in contact with the Ni layer on the component side, the first phase to form is $(\text{Cu},\text{Ni})_6\text{Sn}_5$ —not the Ni_3Sn_4 typically seen with SnPb solders. This is not immediately obvious, as pure Ni_3Sn_4 is much more stable (the standard Gibbs energy of the formation is higher) than pure Cu_6Sn_5 .

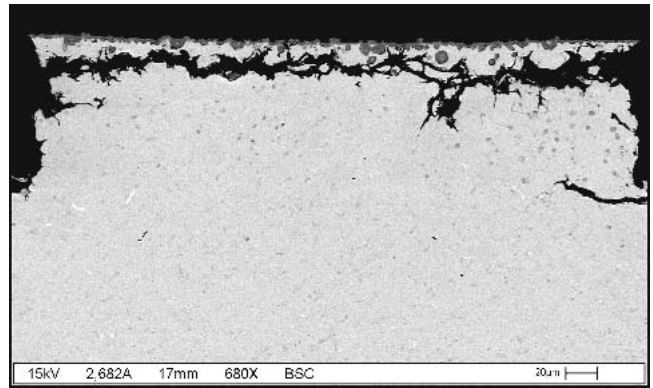


FIG. 6. SEM micrograph of a typical failure path in CSPs soldered on Ni(P)|Au-coated PWB.

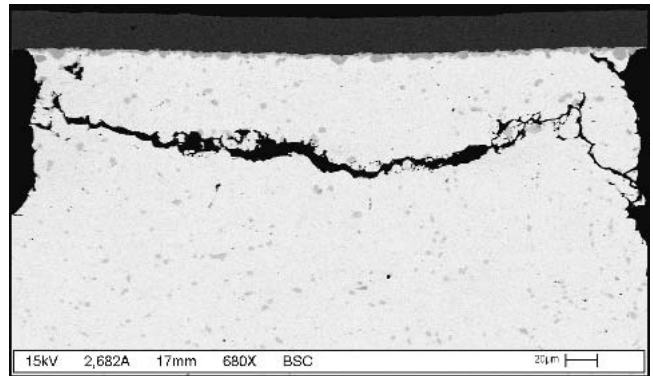


FIG. 7. SEM micrograph of a typical failure path in CSPs soldered on OSP-coated PWB.

However, it has been frequently shown experimentally that even small amounts of Cu in the solder prevents the formation of Ni_3Sn_4 , and $(\text{Cu},\text{Ni})_6\text{Sn}_5$ is formed instead. The reaction from the supersaturated melt is driven by the total Gibbs energy of formation that contains, in addition to the standard Gibbs energy of reaction, the effect of the activities of the reacting species. Therefore the small amount of dissolved Ni in the solder efficiently stabilizes the formation of $(\text{Cu},\text{Ni})_6\text{Sn}_5$.²⁰ Hence, the component-side interface of the solder interconnections is structurally the same for the two substrates. However, the intermetallic compound (IMC) layer formed on the PWB side at the assembly reflow is different: pure Cu_6Sn_5 in the case of Cu|OSP boards and $(\text{Cu},\text{Ni})_6\text{Sn}_5$ in the case of Ni(P)|Au boards.

Optical and scanning electron microscopy revealed distinct differences between the microstructures of the solder interconnections in the Cu|OSP and Ni(P)|Au assemblies. Relative to Ni(P)|Au, interconnections formed on the Cu|OSP boards contained more and larger Cu_6Sn_5 intermetallic particles dispersed in the bulk solder. Differences were also observed in the thickness of the IMC layers on the component side. In the case of Cu pads the layer thickness was about 3–4 μm , whereas in the case of Ni pads it was only about 1.5–3 μm .

As noted above, in addition to the solder paste, the liquid bumps are further alloyed by the dissolving metallizations. The dissolution of Cu in SnPb solders is known to be fairly high as compared with other typical coating materials such as Ni and Pd. The extent of Cu dissolution from the soldering pads was measured in cross-sectional samples by FE-SEM. For the given reflow profile, bump volume, and interconnection composition, an average thickness of $2.7 \mu\text{m}$ ($\delta = 0.63$; $n = 30$) of Cu was dissolved. The amount of Ni dissolution was too small to be detected by FE-SEM. The dissolution rate of Cu in SnPb at 250°C determined experimentally by Bader¹⁶ was about $0.15 \mu\text{m/s}$, whereas that of Ni was only $0.003 \mu\text{m/s}$. Because the dissolution rates depend on the solubilities of the elements (Cu and Ni) in the solder alloys, the same relative difference in dissolution rates was expected with the SnAgCu as Bader found with SnPb (60/40) solder. Thus, Ni dissolution into the SnAgCu interconnection was assumed to be insignificant and that practically all the Ni that dissolves would be bonded into the $(\text{Cu,Ni})_6\text{Sn}_5$ layer at the interface. Cu dissolution rate of $0.07 \mu\text{m/s}$ was calculated based on the measured amount of Cu dissolution and about 40 s time-above-liquidus during the reflow. The dissolution rate calculated for the CSP interconnection was thus about one half of that measured by Bader with the SnPb. The difference probably results from the following: (i) the alloy initially contained Cu, (ii) the dissolution rate depends on both the formation of intermetallic compounds at the dissolving interface and mixing of the liquid solder, and (iii) the small interconnections are rapidly saturated.

The nominal composition of the interconnections on Cu pads was calculated by assuming complete stencil opening filling, perfect paste release, and mixing of the bump and paste material during the reflow soldering. For the given solder interconnection volume, the measured amount of Cu dissolution in the entire area of the soldering pad is enough to raise the Cu concentration in the soldered interconnection close to 1.0 wt% (point O in Fig. 4) even when the amount of Cu bonded in the IMC layers on both sides of the interconnections is taken into account. The nominal composition of the interconnections soldered on Ni(P)|Au pads was calculated in the same manner. Even though the stable solubility of Ni in Cu_6Sn_5 is only about 4 at.%,²¹ the metastable solubility can be as high as 20 at.%.²⁰ Nearly as high Ni content (19 at.%) in the $(\text{Cu,Ni})_6\text{Sn}_5$ was measured by EDS. Thus, taking into account the amount of Cu bonded in the IMC layers on both sides of the interconnections, the nominal composition of the interconnections soldered on the Ni(P)|Au coated pads is about Sn0.5Ag0.3Cu (point N in Fig. 4).

An important consequence of higher Cu content is that the solidification process is different in the interconnections soldered on Ni from those soldered on Cu. It is very

useful to first examine the solidification of solder interconnections with the help of equilibrium phase diagrams. It should be noted, however, that the equilibrium diagrams do not contain information about either the effect of cooling rate or the morphology of the phases. The solidification structures are examined as equilibrium solidification. Figure 8 presents the phase fraction diagrams (NP), where the relative amounts of different phases are presented as a function of temperature.¹⁸ Note that there are two diagrams superimposed. The interconnections soldered on the Ni(P)|Au boards have the final nominal composition of Sn0.5Ag0.3Cu, whereas the interconnections soldered on Cu|OSP have Sn0.5Ag0.9Cu. According to the dashed lines in Fig. 8, the solidification of the liquid interconnections soldered on Ni(P)|Au boards starts with the formation of primary Sn phase when the interconnections are cooled down from the peak reflow temperature to below the liquidus temperature of 229°C . The Cu_6Sn_5 phase nucleates only until below 222°C , where the composition of the liquid reaches the curve of 2-fold saturation, that is, the eutectic valley (see also M in Fig. 4). The solid lines in Fig. 8 presents the phase fraction of Cu_6Sn_5 in the system with the nominal composition of Sn0.5Ag0.9Cu. In this case, the solidification begins with the formation of primary Cu_6Sn_5 below 229°C . However, the nominal composition of the liquid soon meets the curve of two-face saturation, after which the solidification of the interconnections proceeds by the binary eutectic reaction liquid (L) \rightarrow solid eutectic tin $[(\text{Sn})_{\text{eut}}]$ + solid eutectic Cu_6Sn_5 intermetallic compound $[(\text{Cu}_6\text{Sn}_5)_{\text{eut}}]$ Fig. 4). Below the four-phase invariant temperature, there is more than three times as much Cu_6Sn_5 in the Cu|OSP interconnections as in those on the Ni(P)|Au substrate.

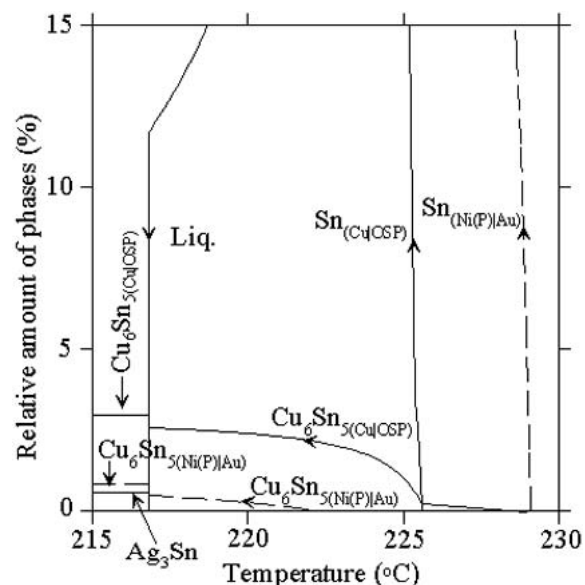


FIG. 8. Combined NP diagram of systems with nominal composition Sn0.5Ag0.3Cu (dashed lines) and Sn0.5Ag0.9Cu (solid lines).¹⁸

The cooling rate used in the reflow process is normally much faster than the rate assumed in equilibrium considerations. Higher cooling rates will eventually evoke under-cooling and more refined microstructures. In practice, then, the solidification process departs somewhat from that of equilibrium solidification. It should be noted that all the microstructures discussed and compared in the following were manufactured with the use of the solder paste P₂. Thus the reflow profile, including the cooling rate, was the same for all samples. The only difference is the coating material on the soldering pads and the subsequent change in the solder compositions. Figure 9 shows an example of the characteristic microstructure formed in the interconnections on Ni(P)|Au soldering pads. Under the reflow conditions used, a cellular structure is generated in which small Cu₆Sn₅ and Ag₃Sn phases are dispersed between large primary Sn cells. Both the Cu₆Sn₅ and the Ag₃Sn particles are uniformly distributed around the relatively large Sn cells. Figure 10 shows the characteristic microstructure of a sample soldered on Cu|OSP. The cellular structure is again visible, although the amount and morphology of the Cu₆Sn₅ phase is different. There is a large amount of primary Cu₆Sn₅ in the microstructure, as was expected from phase diagrams. In addition, numerous small Cu₆Sn₅ particles formed in the binary solidification, are embedded at the boundaries between relatively small Sn cells. Furthermore, the relatively large areas of ternary eutectic structure between the Sn cells indicate that the composition of the liquid moves a greater distance along the eutectic valley in the case of the Cu|OSP pads than in the case of Ni(P)|Au pads.

As described above, the microstructure after reflow in the interconnections on Cu pads is more refined than that on Ni(P)|Au and, based on that one would expect the former are expected to be stronger. At first glance it may seem inconsistent that the Cu|OSP assemblies should fail earlier in thermal cycling. In fact, the performance on the two types of assemblies is related to microstructural

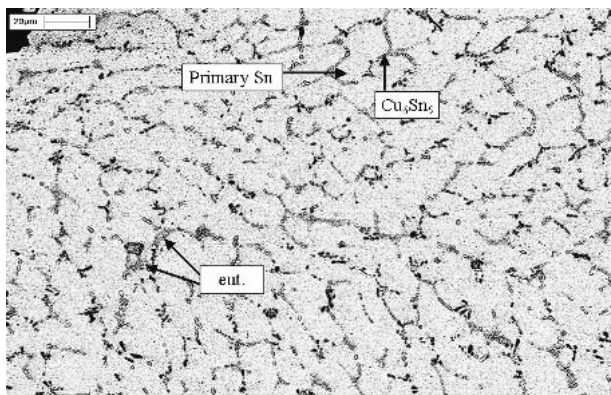


FIG. 9. Microstructure of interconnections on Ni(P)|Au-coated soldering pads, where the nominal composition is Sn0.5Ag0.3Cu.

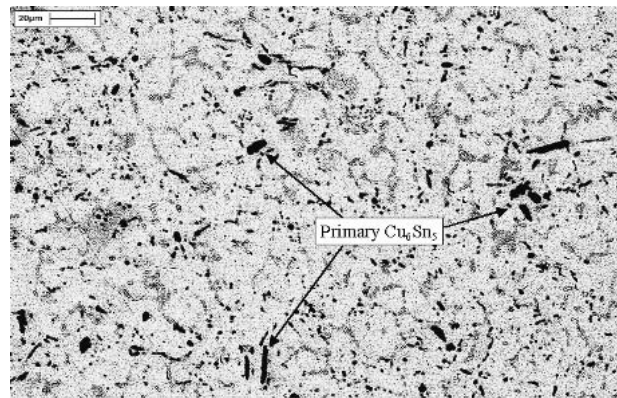


FIG. 10. Microstructure of the interconnections on OSP-coated soldering pads, where the nominal composition is Sn0.5Ag0.9Cu.

changes that occur during the testing. The evolution of microstructures during the thermal tests was studied by optical microscopy with polarized light. Polarized light is useful because the reflection is dependent on the grain orientation of the surface and therefore areas with different orientation are seen in different colors.

Micrographs (a)–(f) in Fig. 11 show how the microstructures evolve due to the deformation-induced recrystallization. Micrographs (a) and (b) show the initial structure of the Ni(P)|Au and Cu|OSP interconnections after reflow soldering. The structure is essentially the same in the two interconnections except for the differences discussed above. The boundaries between the contrasting areas as seen with polarized light are boundaries of colonies of uniformly oriented small Sn cells. (Mechanical twins observed in interconnections stressed with very fast deformation rates conform that the boundaries between the colonies are high angle boundaries. Results from this work will be published later on.) The original interconnections (after reflow) consist of relatively few colonies inside of which the cellular structure is visible. AuSn₄ is typically seen at the boundaries between the colonies. This can be explained as follows: Cu₆Sn₅ and Sn start to solidify when the temperature falls below 229 °C, as noted above. However, AuSn₄ cannot form at such high temperatures. In addition, the solubility of Au in solid Sn is rather small, which leaves Au enriched in the liquid. Thus, AuSn₄ forms only after the temperature falls below 217 °C, as the remaining liquid solidifies.

Micrographs (c) and (d) in Fig. 11 exemplify how the microstructures evolve. In the interconnection soldered on Cu|OSP [Fig. 11(d)], recrystallization is apparent in the entire “neck region” of the interconnection, whereas the rest of the interconnection seems to be mostly unaffected. Recrystallization is also evident in the Ni(P)|Au interconnection [Fig. 11(c)], but it is more localized close to the component side interface of the interconnection. The structure below the recrystallized region in the Ni(P)|Au interconnection has changed as well, most

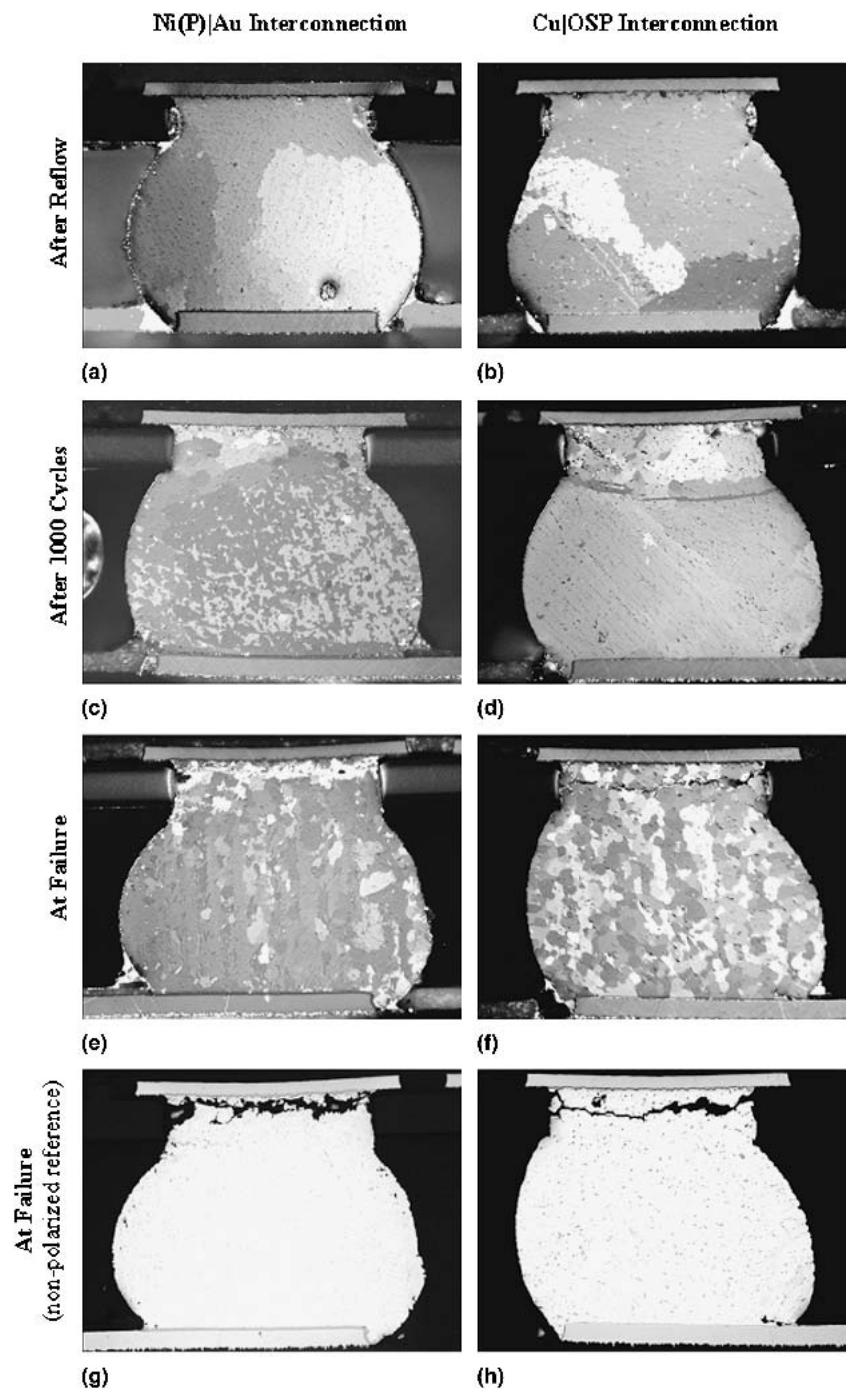


FIG. 11. Evolution of microstructures in Ni(P)|Au and Cu|OSP interconnections during thermal cycling.

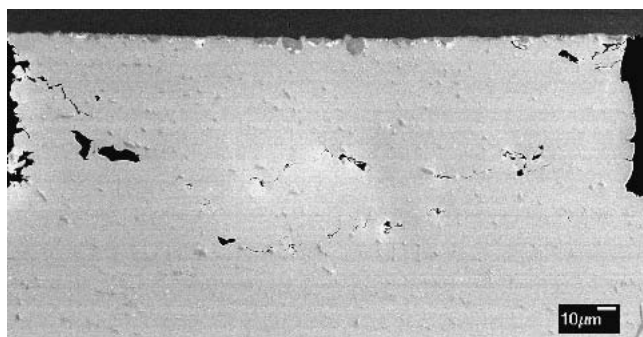
likely due to local coalescence of the Sn cells. The micrographs in Figs. 11(e) and 11(f), depicting the microstructures after the interconnections have failed, show that the kinetic of recrystallization is more rapid in Cu|OSP than in Ni(P)|Au interconnections. Because the major difference in the microstructures of the two interconnections is related to the existence of large primary Cu_6Sn_5 particles in the Cu|OSP interconnections, it is

evident that these particles enhance the nucleation of the recrystallization in the Cu|OSP interconnections. The recrystallization occurs first near the corner region of the interconnections, where the structure is most heavily deformed plastically. It has been previously demonstrated that the second phase particles can accelerate the nucleation of recrystallization in common structural metals.^{23,24} These noncoherent high-angle boundaries

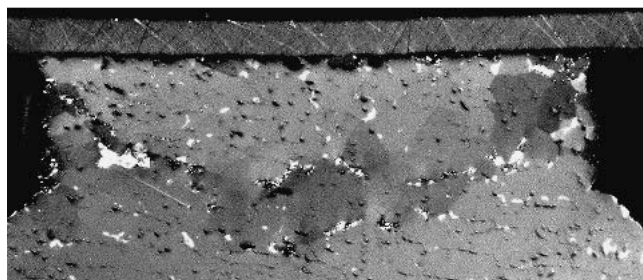
between large Cu_6Sn_5 crystals and solder matrix provide good nucleation sites for the recrystallization, and therefore the rate is faster in the Cu|OSP interconnections.

It is emphasized that the original microstructure of the solder interconnections after the reflow contain, as discussed above, only very few large colonies with high-angle boundaries between them.²⁵ These high-angle boundaries are rarely running parallel to component metallizations or board pads, and therefore they cannot provide potential sites for cracks to nucleate and propagate. If a crack could nucleate in such a solidification structure, they should propagate through the colonies in a very ductile manner. However, the plastic deformation occurring during thermal cycling tests, especially in the neck regions of solder interconnections, provides the driving force needed for the recrystallization of the solidification structure. It is the gradual expansion of the recrystallized structure from the corner regions of the interconnections that creates the grain boundaries and so makes the intergranular fracture of the interconnections possible.

The failure analyses carried out on the samples tested only until 1000 cycles (before electrical failure) supports this interpretation: the cracks do not nucleate only at the corners of the interconnection, as seen in Fig. 12(a), but they also nucleate and grow at the boundaries between the recrystallized part and the non-recrystallized part, as seen in Fig. 12(b). This, together with the earlier discussion of the difference in the rate of recrystallization, explains why the fractures in Ni(P)|Au interconnections



(a)



(b)

FIG. 12. Crack nucleation at the boundaries between recrystallized grains and the non-recrystallized part of the interconnections (Cu|OSP).

typically locate closer to the component-side interface, whereas the Cu|OSP interconnections generally located farther away in the solder/metallization interface. Furthermore, because the kinetics of recrystallization of the interconnections on Cu|OSP is faster, cracks can also nucleate and propagate more rapidly and therefore the interconnections on Cu|OSP will fail earlier.

IV. CONCLUSIONS

The reliability of the CSP components soldered on the Ni(P)|Au-finished boards was significantly better than that of the components soldered on OSP-finished boards. The kinetics of recrystallization was observed to control the reliability performance of solder interconnections under thermomechanical loading. The interconnections on Cu|OSP recrystallized faster than those on Ni(P)|Au pads. This is due to the primary Cu_6Sn_5 particles dispersed in the solder matrix of the Cu|OSP interconnections. The primary particles decrease the incubation time for the recrystallization by providing favorable nucleation sites for the recrystallization. Because the recrystallization proceeds faster in the Cu|OSP interconnections, the cracks can also nucleate and propagate faster and so they fail earlier. The formation of continuous network of grain boundaries is needed for the cracks to grow through the neck regions of the solder interconnections.

The difference in the rate of recrystallization reflects the differences in bulk microstructures of the solder interconnections. In the case of Ni(P)|Au assemblies, the microstructure of the solder interconnections is composed of primary tin cells between which the binary and ternary eutectic structures are embedded. In this microstructure, the volume fraction of the nearly pure primary tin is more than 98 vol%. In contrast, during the reflow soldering of the Cu|OSP assemblies, liquid solder interconnections become significantly enriched by copper from the board pads, and the solidification of the liquid interconnections leads to a different microstructure. In this case, solidification starts with precipitation of primary Cu_6Sn_5 particles and continues with simultaneous formation of the binary eutectic Sn and Cu_6Sn_5 phases, which generates a more heterogeneous microstructure than that of the Ni(P)|Au assemblies.

The results of thermal cycling tests showed that there are no statistically significant differences in reliability between the CSP components soldered with the different near-eutectic SnAgCu solder pastes. This is due to the fact that the solder bump material largely determines the compositions of the solder interconnections after the reflow.

ACKNOWLEDGMENTS

The authors wish to thank Dr. Tomi Laurila for valuable discussions and his help in completing the manuscript. The help of Dr. Erkki Heikinheimo and Dr. Kari

Lounatmaa in the SEM studies is greatly appreciated. We are also indebted to the National Technology Agency of Finland and the Finnish electronics industry for their financial support.

REFERENCES

1. J.K. Kivilahti and K. Kulojärvi: In *Design and Reliability of Solders and Solder Interconnections*, edited by R.K. Mahidhara (TMS, Warrendale, PA, 1997), pp. 377–384.
2. V. Puligandla, S. Dunford, and J.K. Kivilahti: In *Handbook of Lead(Pb)-Free Technology for Microelectronics Assemblies*, edited by K. Puttliz and K. Stalter (Marcel Dekker Inc., New York, 2004), p. 1026
3. J.E. Sohn: Are lead-free solder joints reliable? *Circuits Assembly June*, 32 (2002).
4. A. Syed: Reliability and Au Embrittlement of Lead Free Solders for BGA Applications. *2001 International Symposium on Advanced Packaging Materials*, pp. 143–147.
5. M. Amagai: Characterization of chip scale packaging materials. *Microelectronics Reliability* **39**, 1365 (1999).
6. Z.P. Wang, Y.M. Tan, and K.M. Chua: Board level reliability assessment of chip scale packages. *Microelectronics Reliability* **39**, 1351 (1999).
7. S.R. Lee, B.H.W. Lui, Y.H. Kong, B. Baylon, T. Leung, P. Umali, and H. Ahtarap: Assessment of board level solder joint reliability for PBGA assemblies with lead-free solder joints. *Soldering and Surface Mount* **14**, 46 (2002).
8. E. Bradley and K. Banerji: Effect of PCB Finish on the Reliability and Wettability of Ball Grid Array Packages. *IEEE Transactions on Components, Packaging and Manufacturing Technology* **19**, 320 (1996).
9. T. Hirano, K. Fukuda, K. Ito, T. Kiga, and Y. Taniguchi: Reliability of Lead Free Solder Joint by Using Chip Size Package. *Electronics and the Environment. Proceedings of the 2001 IEEE International Symposium*, Piscataway, NJ, pp. 285–289.
10. P.T. Vianco: An overview of surface finishes and their role in printed circuit board solderability and solder joint performance. *Soldering and Surface Mount* **25**, 6 (1998).
11. K. Kulojärvi and J.K. Kivilahti: Effect of Dissolution and intermetallic formation on the reliability of flip chip joints—comparison between Cu and Ni. *Microelectronics International* **15**, 20 (1998).
12. S.K. Kang, D.Y. Shih, K. Fogel, P. Lauro, M.J. Yim, G. Advocate, M. Griffin, C. Goldsmith, D.W. Henderson, T. Gosselin, D. King, J. Konrad, A. Sarkhel, and K.J. Puttliz: Interfacial Reaction Studies on Lead (Pb)-Free Solder Alloys. *Electronic Components and Technology Conference 2001*. Institute of Electrical and Electronics Engineers, Piscataway, NJ.
13. J. Sigelko, S. Choi, K.N. Subramanian, and J.P. Lucas: The effect of small additions of copper on the aging kinetics of the intermetallic layer and intermetallic particles of eutectic tin-silver solder joints. *Journal of Electric Materials* **29**, 1307 (2000).
14. C.E. Ho, R.Y. Tsai, Y.L. Lin, and C.R. Kao: Effect of Cu concentration on the reactions between Sn-Ag-Cu solders and Ni. *Journal of Electronic Materials* **31**, 584 (2002).
15. W.G. Bader: Dissolution and Formation on Intermetallics in the Soldering Process. *Proceedings of the Conference on Physical Metallurgy and Metal Joining*, edited by R. Kossowsky and M.F. Glicksman (TMS/AIME, Warrendale, PA, 1980).
16. W.G. Bader: Dissolution of Au, Ag, Pd, Pt, Cu and Ni in a molten Sn-lead solder. *Welding Journal* **48**, 551 (1969).
17. S. Chada, R.A. Fournelle, W. Laub, and D. Shangguan: Copper substrate dissolution in eutectic Sn-Ag solder and its effect on microstructure. *J. Electron. Mater.* **29**, 1214 (2000).
18. “IPMA”—The Thermodynamic Databank for Interconnection and Packaging Materials. Helsinki University of Technology, Helsinki (2001).
19. P. O’Connor: *Practical Reliability Engineering*, 3rd ed. (John Wiley & Sons Ltd., West Sussex, 1991) p. 431.
20. K. Zeng, V. Vuorinen, and J.K. Kivilahti: Intermetallic Reactions between Lead-free SnAgCu Solder and Ni(P)/Au Finish on PWB. *Proceedings of the 51st Electronic Components and Technology Conference*, edited by John Lau. (Institute of Electrical and Electronics Engineers, Piscataway, NJ, 2001) pp. 693–698.
21. P. Oberndorff: Ph.D. Thesis. Eindhoven University of Technology, The Netherlands (2001).
22. W. Peng, K. Zeng, and J.K. Kivilahti: Potential Pb-free Solder Systems. Report Series TTK-EVT-1. (Helsinki University of Technology, Helsinki, 2000).
23. W.C. Leslie, T.J. Michalak, and F.W. Aul: In *Iron and Its Dilute Solid Solutions*, edited by C.W. Spencer and F.E. Werner (Interscience Publishers, New York, 1963).
24. R.W. Cahn: *Physical Metallurgy* (NH Physics, Amsterdam, 1965).
25. J. Koivisto: M.S. Thesis. Helsinki University of Technology (2004).